Supersymmetric QCD corrections to Higgs-b production: Is the Δ_b approximation accurate?

S. Dawson,[1] C. B. Jackson,[2] and P. Jaiswal[1,3]

[1]*Department of Physics, Brookhaven National Laboratory, Upton, New York 11973, USA*
[2]*Physics Department, University of Texas, Arlington, Texas*
[3]*Yang Institute for Theoretical Physics, Stony Brook University, Stony Brook, New York 11790, USA*

(Received 11 April 2011; published 8 June 2011)

The associated production of a Higgs boson with a b quark is a discovery channel for the lightest MSSM neutral Higgs boson. We consider the supersymmetric QCD contributions from squarks and gluinos and discuss the decoupling properties of these effects. A detailed comparison of our exact $\mathcal{O}(\alpha_s)$ results with those of a widely used effective Lagrangian approach, the Δ_b approximation, is presented. The Δ_b approximation is shown to accurately reproduce the exact one-loop supersymmetric QCD result to within a few percent over a wide range of parameter space.

DOI: 10.1103/PhysRevD.83.115007 PACS numbers: 13.85.−t, 14.80.Da

I. INTRODUCTION

Once a light Higgs-like particle is discovered it will be critical to determine if it is the Higgs boson predicted by the standard model. The minimal supersymmetric standard model (MSSM) presents a comparison framework in which to examine the properties of a putative Higgs candidate. The MSSM Higgs sector contains five Higgs bosons–two neutral bosons, h and H, a pseudoscalar boson, A, and two charged bosons, $H^{\pm}$. At the tree level the theory is described by just two parameters, which are conveniently chosen to be M_A, the mass of the pseudoscalar boson, and $\tan\beta$, the ratio of vacuum expectation values of the two neutral Higgs bosons. Even when radiative corrections are included, the theory is highly predictive [1–3].

In the MSSM, the production mechanisms for the Higgs bosons can be significantly different from those in the standard model. For large values of $\tan\beta$, the heavier Higgs bosons, A and H, are predominantly produced in association with b quarks. Even for $\tan\beta \sim 5$, the production rate in association with b quarks is similar to that from gluon fusion for A and H production [4]. For the lighter Higgs boson h, for $\tan\beta 4 \gtrsim 7$, the dominant production mechanism at both the Tevatron and the LHC is production with b quarks for light M_A ($\lesssim 200$ GeV), where the $b\bar{b}h$ coupling is enhanced. Both the Tevatron [5] and the LHC experiments [6] have presented limits for Higgs production in association with b quarks, searching for the decays $h \to \tau^+\tau^-$ and $b\bar{b}$.[1] These limits are obtained in the context of the MSSM and are sensitive to the b-squark and gluino loop corrections which we consider here.

The rates for bh associated production at the LHC and the Tevatron have been extensively studied[9–19], and the next-to-leading order (NLO) QCD corrections are well understood, both in the four-flavor and five-flavor number parton schemes (4FNS and 5FNS, respectively) [10,12,16]. In the four-flavor number scheme, the lowest order processes for producing a Higgs boson and a b quark are $gg \to b\bar{b}h$ and $q\bar{q} \to b\bar{b}h$ [9,13,18]. In the five-flavor number scheme, the lowest order process is $bg \to bh$ ($\bar{b}g \to \bar{b}h$). The two schemes represent different orderings of perturbation theory, and calculations in the two schemes produce rates which are in qualitative agreement [4,12]. In this paper, we use the five-flavor number scheme for simplicity. The resummation of threshold logarithms [20], electroweak corrections [21,22], and supersymmetric (SUSY) QCD corrections [23] have also been computed for bh production in the five-flavor number scheme.

Here, we focus on the role of squark and gluino loops. The properties of the SUSY QCD (SQCD) corrections to the $b\bar{b}h$ vertex, both for the decay $h \to b\bar{b}$ [24–27] and the production $b\bar{b} \to h$ [13,27–29], were computed long ago. The contributions from b squarks and gluinos to the lightest MSSM Higgs boson mass are known at two loops [30,31], while the two-loop SQCD contributions to the $b\bar{b}h$ vertex are known in the limit in which the Higgs mass is much smaller than the squark and gluino masses [32,33]. The contributions of squarks and gluinos to the on-shell $b\bar{b}h$ vertex are nondecoupling for heavy squark and gluino masses, and decoupling is only achieved when the pseudoscalar mass M_A also becomes large.

An effective Lagrangian approach, the Δ_b approximation [25,26], can be used to approximate the SQCD contributions to the on-shell $b\bar{b}h$ vertex and to resum the $(\alpha_s \tan\beta/M_{\mathrm{SUSY}})^n$ enhanced terms. The numerical accuracy of the Δ_b effective Lagrangian approach has been examined for a number of cases. The two-loop contributions to the lightest MSSM Higgs boson mass of $\mathcal{O}(\alpha_b\alpha_s)$ were computed in Refs. [30,31], and it was found that the majority of these corrections could be absorbed into a one-loop contribution by defining an effective b-quark mass using the Δ_b approach. The subleading contributions to the Higgs boson mass (those not absorbed into Δ_b) are then of $\mathcal{O}(1\ \mathrm{GeV})$. The Δ_b approach also yields an excellent approximation to the SQCD corrections for the decay process

[1]The expected sensitivities of ATLAS and CMS to b Higgs associated production are described in Refs. [7,8].

$h \to b\bar{b}$ [27]. It is particularly interesting to study the accuracy of the Δ_b approximation for production processes where one of the b quarks is off shell. The SQCD contributions from squarks and gluinos to the inclusive Higgs production rate in association with b quarks have been studied extensively in the 4FNS in Ref. [34], where the lowest order contribution is $gg \to b\bar{b}h$. In the 4FNS, the inclusive cross section, including the exact one-loop SQCD corrections, is reproduced to within a few percent using the Δ_b approximation. However, the accuracy of the Δ_b approximation for the MSSM neutral Higgs boson production in the 5FNS has been studied for only a small set of MSSM parameters in Ref. [23]. The major new result of this paper is a detailed study of the accuracy of the Δ_b approach in the 5FNS for the $bg \to bh$ production process. In this case, one of the b quarks is off shell and there are contributions which are not contained in the effective Lagrangian approach.

The plan of the paper is as follows: Sec. II contains a brief review of the MSSM Higgs and b-squark sectors and also a review of the effective Lagrangian approximation. The calculation of Ref. [23] is summarized in Sec. II. We include SQCD contributions to bh production that are enhanced by $m_b \tan\beta$, which were omitted in Ref. [23]. Analytic results for the SQCD corrections to $bg \to bh$ in the extreme mixing scenarios in the b-squark sector are presented in Sec. III. Section IV contains numerical results for the $\sqrt{s} = 7$ TeV LHC. Finally, our conclusions are summarized in Sec. V. Detailed analytic results are relegated to a series of appendixes.

II. BASICS

A. MSSM framework

In the simplest version of the MSSM there are two Higgs doublets, H_u and H_d, which break the electroweak symmetry and give masses to the W and Z gauge bosons. The neutral Higgs boson masses are given at tree level by

$$M_{h,H}^2 = \frac{1}{2}\left[M_A^2 + M_Z^2 \mp \sqrt{(M_A^2 + M_Z^2)^2 - 4M_A^2 M_Z^2 \cos^2 2\beta}\right], \tag{1}$$

and the angle α which diagonalizes the neutral Higgs mass is

$$\tan 2\alpha = \tan 2\beta \left(\frac{M_A^2 + M_Z^2}{M_A^2 - M_Z^2}\right). \tag{2}$$

In practice, the relations of Eqs. (1) and (2) receive large radiative corrections which must be taken into account in numerical studies. We use the program FEYNHIGGS [35–37] to generate the Higgs masses and an effective mixing angle, α_{eff}, which incorporates higher order effects.

The scalar partners of the left- and right-handed b quarks, $\tilde{b}_L$ and $\tilde{b}_R$, are not mass eigenstates, but mix according to

$$L_M = -(\tilde{b}_L^*, \tilde{b}_R^*) M_{\tilde{b}}^2 \begin{pmatrix} \tilde{b}_L \\ \tilde{b}_R \end{pmatrix}. \tag{3}$$

The $\tilde{b}$-squark mass matrix is

$$M_{\tilde{b}}^2 = \begin{pmatrix} \tilde{m}_L^2 & m_b X_b \\ m_b X_b & \tilde{m}_R^2 \end{pmatrix}, \tag{4}$$

and we define

$$\begin{aligned} X_b &= A_b - \mu \tan\beta, \\ \tilde{m}_L^2 &= M_Q^2 + m_b^2 + M_Z^2 \cos 2\beta (I_3^b - Q_b \sin^2\theta_W), \\ \tilde{m}_R^2 &= M_D^2 + m_b^2 + M_Z^2 \cos 2\beta Q_b \sin^2\theta_W. \end{aligned} \tag{5}$$

$M_{Q,D}$ are the soft SUSY breaking masses, $I_3^b = -1/2$, and $Q_b = -1/3$. The parameter A_b is the trilinear scalar coupling of the soft supersymmetry breaking Lagrangian and μ is the Higgsino mass parameter. The b-squark mass eigenstates are $\tilde{b}_1$ and $\tilde{b}_2$, and they define the b-squark mixing angle $\tilde{\theta}_b$,

$$\begin{aligned} \tilde{b}_1 &= \cos\tilde{\theta}_b \tilde{b}_L + \sin\tilde{\theta}_b \tilde{b}_R, \\ \tilde{b}_2 &= -\sin\tilde{\theta}_b \tilde{b}_L + \cos\tilde{\theta}_b \tilde{b}_R. \end{aligned} \tag{6}$$

At tree level,

$$\sin 2\tilde{\theta}_b = \frac{2m_b(A_b - \mu \tan\beta)}{M_{\tilde{b}_1}^2 - M_{\tilde{b}_2}^2} \tag{7}$$

and the sbottom mass eigenstates are

$$M_{\tilde{b}_1,\tilde{b}_2}^2 = \frac{1}{2}\left[\tilde{m}_L^2 + \tilde{m}_R^2 \mp \sqrt{(\tilde{m}_L^2 - \tilde{m}_R^2)^2 + 4m_b^2 X_b^2}\right]. \tag{8}$$

B. Δ_b approximation: The effective Lagrangian approach

Loop corrections which are enhanced by powers of $\alpha_s \tan\beta$ can be included in an effective Lagrangian approach. At tree level, there is no $\bar{\psi}_L b_R H_u$ coupling in the MSSM, but such a coupling arises at one loop and gives an effective interaction [25–27],[2]

$$L_{\text{eff}} = -\lambda_b \bar{\psi}_L \left(H_d + \frac{\Delta_b}{\tan\beta} H_u\right) b_R + \text{H.c.} \tag{9}$$

Equation (9) shifts the b-quark mass from its tree-level value[3]

$$m_b \to \frac{\lambda_b v_1}{\sqrt{2}}(1 + \Delta_b), \tag{10}$$

and also implies that the Yukawa couplings of the Higgs bosons to the b quark are shifted from the tree-level

[2] The neutral components of the Higgs bosons receive vacuum expectation values: $\langle H_d^0 \rangle = \frac{v_1}{\sqrt{2}}$, $\langle H_u^0 \rangle = \frac{v_2}{\sqrt{2}}$.

[3] $v_{\text{SM}} = (\sqrt{2}G_F)^{-1/2}$, $v_1 = v_{\text{SM}} \cos\beta$.

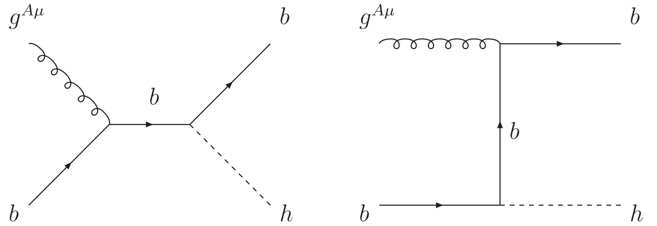

FIG. 1. Feynman diagrams for $g(q_1) + b(q_2) \to b(p_b) + h(p_h)$.

predictions. This shift of the Yukawa couplings can be included with an effective Lagrangian approach [26,27],

$$L_{\rm eff} = -\frac{m_b}{v_{\rm SM}}\left(\frac{1}{1+\Delta_b}\right)\left(-\frac{\sin\alpha}{\cos\beta}\right)\left(1 - \frac{\Delta_b}{\tan\beta\tan\alpha}\right)\bar{b}bh. \tag{11}$$

The Lagrangian of Eq. (11) has been shown to sum all terms of $\mathcal{O}(\alpha_s \tan\beta)^n$ for large $\tan\beta$ [25,26].[4] This effective Lagrangian has been used to compute the SQCD corrections to both the inclusive production process $b\bar{b} \to h$ and the decay process $h \to b\bar{b}$, and yields results which are within a few percent of the exact one-loop SQCD calculations [27,34].

The expression for Δ_b is found in the limit $m_b \ll M_h$, $M_Z \ll M_{\tilde{b}_1}$, $M_{\tilde{b}_2}$, $M_{\tilde{g}}$. The one-loop contribution to Δ_b from sbottom/gluino loops is [25,26,38]

$$\Delta_b = \frac{2\alpha_s(\mu_S)}{3\pi} M_{\tilde{g}}\mu \tan\beta I(M_{\tilde{b}_1}, M_{\tilde{b}_2}, M_{\tilde{g}}), \tag{12}$$

where the function $I(a, b, c)$ is

$$I(a,b,c) = \frac{1}{(a^2-b^2)(b^2-c^2)(a^2-c^2)}\left\{a^2b^2\log\left(\frac{a^2}{b^2}\right) + b^2c^2\log\left(\frac{b^2}{c^2}\right) + c^2a^2\log\left(\frac{c^2}{a^2}\right)\right\}, \tag{13}$$

and $\alpha_s(\mu_S)$ should be evaluated at a typical squark or gluino mass. The two-loop QCD corrections to Δ_b have been computed and demonstrate that the appropriate scale at which to evaluate Δ_b is indeed of the order of the heavy squark and gluino masses [32,33]. The renormalization scale dependence of Δ_b is minimal around $\mu_0/3$, where $\mu_0 \equiv (M_{\tilde{g}} + m_{\tilde{b}_1} + m_{\tilde{b}_2})/3$. In our language this is a high scale, of order the heavy SUSY particle masses. The squarks and gluinos are integrated out of the theory at this high scale, and their effects are contained in Δ_b. The effective Lagrangian is then used to calculate light Higgs production at a low scale, which is typically the electroweak scale, ~100 GeV.

Using the effective Lagrangian of Eq. (9), which we term the improved Born approximation (or Δ_b approximation), the cross section is written in terms of the effective coupling,

$$g_{bbh}^{\Delta_b} \equiv g_{bbh}\left(\frac{1}{1+\Delta_b}\right)\left(1 - \frac{\Delta_b}{\tan\beta\tan\alpha}\right), \tag{14}$$

where

$$g_{bbh} = -\left(\frac{\sin\alpha}{\cos\beta}\right)\frac{\bar{m}_b(\mu_R)}{v_{\rm SM}}. \tag{15}$$

We evaluate $\bar{m}_b(\mu_R)$ using the two-loop $\overline{\rm MS}$ value at a scale μ_R of $\mathcal{O}(M_h)$, and use the value of $\alpha_{\rm eff}$ determined from FEYNHIGGS. The improved Born approximation consists of rescaling the tree-level cross section σ_0 by the coupling of Eq. (14),[5]

$$\sigma_{\rm IBA} = \left(\frac{g_{bbh}^{\Delta_b}}{g_{bbh}}\right)^2 \sigma_0. \tag{16}$$

The improved Born approximation has been shown to accurately reproduce the full SQCD calculation of $pp \to \bar{t}bH^+$ [39,40].

The one-loop result including the SQCD corrections for $bg \to bh$ can be written as

$$\sigma_{\rm SQCD} \equiv \sigma_{\rm IBA}(1 + \Delta_{\rm SQCD}), \tag{17}$$

where $\Delta_{\rm SQCD}$ is found from the exact SQCD calculation summarized in Appendix B.

The improved Born approximation involves making the replacement in the tree-level Lagrangian,

$$m_b \to \frac{m_b}{1+\Delta_b}. \tag{18}$$

Consistency requires that this substitution also be made in the squark mass matrix of Eq. (4) [41,42],

$$M_{\tilde{b}}^2 \to \begin{pmatrix} \tilde{m}_L^2 & \left(\frac{m_b}{1+\Delta_b}\right)X_b \\ \left(\frac{m_b}{1+\Delta_b}\right)X_b & \tilde{m}_R^2 \end{pmatrix}. \tag{19}$$

The effects of the substitution of Eq. (18) in the b-squark mass matrix are numerically important, although they generate contributions which are formally higher order in α_s. Equations (12) and (19) can be solved iteratively for $M_{\tilde{b}_1}$, $M_{\tilde{b}_2}$, and Δ_b using the procedure of Ref. [41].[6]

C. SQCD contributions to $gb \to bh$

The contributions from squark and gluino loops to the $gb \to bh$ process have been computed in Ref. [23] in the $m_b = 0$ limit. We extend that calculation by including terms which are enhanced by $m_b \tan\beta$ and provide analytic results in several useful limits.

[4]It is also possible to sum the contributions which are proportional to A_b, but these terms are less important numerically [27].

[5]This is the approximation used in Ref. [4] to include the SQCD corrections.

[6]We use FEYNHIGGS only for calculating M_h and $\sin\alpha_{\rm eff}$.

The tree-level diagrams for $g(q_1) + b(q_2) \to b(p_b) + h(p_h)$ are shown in Fig. 1. We define the following dimensionless spinor products:

$$\begin{aligned} M_s^\mu &= \frac{\bar{u}(p_b)(\not{q}_1 + \not{q}_2)\gamma^\mu u(q_2)}{s}, \\ M_t^\mu &= \frac{\bar{u}(p_b)\gamma^\mu(\not{p}_b - \not{q}_1)u(q_2)}{t}, \\ M_1^\mu &= q_2^\mu \frac{\bar{u}(p_b)u(q_2)}{u}, \\ M_2^\mu &= \frac{\bar{u}(p_b)\gamma^\mu u(q_2)}{m_b}, \\ M_3^\mu &= p_b^\mu \frac{\bar{u}(p_b)\not{q}_1 u(q_2)}{m_b t}, \\ M_4^\mu &= q_2^\mu \frac{\bar{u}(p_b)\not{q}_1 u(q_2)}{m_b s}, \end{aligned} \tag{20}$$

where $s = (q_1 + q_2)^2$, $t = (p_b - q_1)^2$, and $u = (p_b - q_2)^2$. In the $m_b = 0$ limit, the tree-level amplitude depends only on M_s^μ and M_t^μ, and M_1^μ is generated at one loop. When the effects of the b mass are included, M_2^μ, M_3^μ, and M_4^μ are also generated.

The tree-level amplitude is

$$\mathcal{A}^{\,a}_{\alpha\beta}|_0 = -g_s g_{bbh}(T^a)_{\alpha\beta}\epsilon_\mu(q_1)\{M_s^\mu + M_t^\mu\}, \tag{21}$$

and the one-loop contribution can be written as

$$\mathcal{A}^{\,a}_{\alpha\beta} = -\frac{\alpha_s(\mu_R)}{4\pi} g_s g_{bbh}(T^a)_{\alpha\beta}\sum_j X_j M_j^\mu \epsilon_\mu(q_1). \tag{22}$$

In the calculations to follow, only the nonzero X_j coefficients are listed and we neglect terms of $\mathcal{O}(m_b^2/s)$ if they are not enhanced by $\tan\beta$.

The renormalization of the squark and gluino contributions is performed in the on-shell scheme and has been described in Refs. [23,32,43]. The bottom quark self-energy is

$$\Sigma_b(p) = \not{p}(\Sigma_b^V(p^2) - \Sigma_b^A(p^2)\gamma_5) + m_b\Sigma_b^S(p^2). \tag{23}$$

The b-quark fields are renormalized as $b \to \sqrt{Z_b^V}b$ and $Z_b^V \equiv \sqrt{1 + \delta Z_b^V}$. The contribution from the counterterms to the self-energy is

$$\begin{aligned} \Sigma_b^{\rm ren}(p) &= \Sigma_b(p) + \delta\Sigma_b(p), \\ \delta\Sigma_b(p) &= \not{p}(\delta Z_b^V - \delta Z_b^A\gamma_5) - m_b\delta Z_b^V - \delta m_b. \end{aligned} \tag{24}$$

Neglecting the γ_5 contribution, the renormalized self-energy is then given by

$$\Sigma_b^{\rm ren}(p) = (\not{p} - m_b)(\Sigma_b^V(p^2) + \delta Z_b^V) + m_b\left(\Sigma_b^S(p^2) + \Sigma_b^V(p^2) - \frac{\delta m_b}{m_b}\right). \tag{25}$$

The on-shell renormalization condition implies

$$\Sigma_b^{\rm ren}(p)|_{\not{p}=m_b} = 0, \tag{26}$$

$$\lim_{\not{p}\to m_b}\left(\frac{\Sigma_b^{\rm ren}(p)}{\not{p} - m_b}\right) = 0. \tag{27}$$

The mass and wave function counterterms are[7]

$$\begin{aligned} \frac{\delta m_b}{m_b} &= [\Sigma_b^S(p^2) + \Sigma_b^V(p^2)]_{p^2=m_b^2} \\ &= \frac{\alpha_s(\mu_R)}{3\pi}\sum_{i=1}^2\left[(-1)^i\frac{M_{\tilde{g}}}{m_b}s_{2\tilde{b}}B_0 - B_1\right](0; M_{\tilde{g}}^2, M_{\tilde{b}_i}^2), \end{aligned} \tag{28}$$

$$\begin{aligned} \delta Z_b^V &= -\Sigma_b^V(p^2)|_{p^2=m_b^2} - 2m_b^2\frac{\partial}{\partial p^2}(\Sigma_b^V(p^2) + \Sigma_S(p^2))|_{p^2=m_b^2} \\ &= \frac{\alpha_s(\mu_R)}{3\pi}\sum_{i=1}^2[B_1 + 2m_b^2B_1' - (-1)^i 2m_b M_{\tilde{g}}s_{2\tilde{b}}B_0'] \\ &\quad \times (0; M_{\tilde{g}}^2, M_{\tilde{b}_i}^2), \end{aligned} \tag{29}$$

where we consistently neglect the b-quark mass if it is not enhanced by $\tan\beta$. The Passarino-Veltman functions $B_0(0; M_{\tilde{g}}^2, M_{\tilde{b}_i}^2)$ and $B_1(0; M_{\tilde{g}}^2, M_{\tilde{b}_i}^2)$ are defined in Appendix A. Using the tree-level relationship of Eq. (7), the mass counterterm can be written as

$$\begin{aligned} \frac{\delta m_b}{m_b} &= \frac{2\alpha_s(\mu_R)}{3\pi}M_{\tilde{g}}A_b I(M_{\tilde{b}_1}, M_{\tilde{b}_2}, M_{\tilde{g}}) - \Delta_b \\ &\quad - \frac{\alpha_s(\mu_R)}{3\pi}\sum_{i=1}^2 B_1(0; M_{\tilde{g}}^2, M_{\tilde{b}_i}^2). \end{aligned} \tag{30}$$

The external gluon is renormalized as $g_\mu^A \to \sqrt{Z_3}g_\mu^A = \sqrt{1 + \delta Z_3}g_\mu^A$ and the strong coupling renormalization is $g_s \to Z_g g_s$ with $\delta Z_g = -\delta Z_3/2$. We renormalize g_s using the $\overline{\rm MS}$ scheme with the heavy squark and gluino contributions subtracted at zero momentum [44],

$$\delta Z_3 = -\frac{\alpha_s(\mu_R)}{4\pi}\left[\frac{1}{6}\Sigma_{\tilde{q}_i}\left(\frac{4\pi\mu_R^2}{M_{\tilde{q}_i}^2}\right)^\epsilon + 2\left(\frac{4\pi\mu_R^2}{M_{\tilde{g}}^2}\right)^\epsilon\right]\frac{1}{\epsilon}\Gamma(1+\epsilon). \tag{31}$$

In order to avoid overcounting the effects which are contained in $g_{bbh}^{\Delta_b}$ to $\mathcal{O}(\alpha_s)$, we need the additional counterterm

$$\delta_{\rm CT} = \Delta_b\left(1 + \frac{1}{\tan\beta\tan\alpha}\right). \tag{32}$$

The total contribution of the counterterms is

[7] $s_{2\tilde{b}} \equiv \sin 2\tilde{\theta}_b$.

$$\sigma_{\rm CT} = \sigma_{\rm IBA}\left(2\delta Z_b^V + \delta Z_3 + 2\delta Z_g + 2\frac{\delta m_b}{m_b} + 2\delta_{\rm CT}\right) = 2\sigma_{\rm IBA}\left(\delta Z_b^V + \frac{\delta m_b}{m_b} + \delta_{\rm CT}\right). \tag{33}$$

The $\tan\beta$ enhanced contributions from Δ_b cancel between Eqs. (30) and (32). The expressions for the contributions to the X_i, as defined in Eq. (22), are given in Appendix B for arbitrary squark and gluino masses, and separately for each one-loop diagram.

III. RESULTS FOR MAXIMAL AND MINIMAL MIXING IN THE b-SQUARK SECTOR

A. Maximal mixing

The squark and gluino contributions to $bg \to bh$ can be examined analytically in several scenarios. In the first scenario,

$$|\tilde{m}_L^2 - \tilde{m}_R^2| \ll \frac{m_b}{1+\Delta_b}|X_b|. \tag{34}$$

We expand in powers of $\frac{|\tilde{m}_L^2 - \tilde{m}_R^2|}{m_b X_b}$. In this case the sbottom masses are nearly degenerate,

$$M_S^2 \equiv \frac{1}{2}[M_{\tilde{b}_1}^2 + M_{\tilde{b}_2}^2],$$
$$|M_{\tilde{b}_1}^2 - M_{\tilde{b}_2}^2| = \left(\frac{2m_b|X_b|}{1+\Delta_b}\right)\left(1 + \frac{(\tilde{m}_L^2 - \tilde{m}_R^2)^2(1+\Delta_b)^2}{8m_b^2X_b^2}\right) \ll M_S^2. \tag{35}$$

This scenario is termed maximal mixing since

$$\sin 2\tilde{\theta}_b \sim 1 - \frac{(\tilde{m}_L^2 - \tilde{m}_R^2)^2(1+\Delta_b)^2}{8m_b^2X_b^2}. \tag{36}$$

We expand the contributions of the exact one-loop SQCD calculation given in Appendix B in powers of $1/M_S$, keeping terms to $\mathcal{O}(\frac{M_{\rm EW}^2}{M_S^2})$ and assuming $M_S \sim M_{\tilde{g}} \sim \mu \sim A_b \sim \tilde{m}_L \sim \tilde{m}_R \gg M_W, M_Z, M_h \sim M_{\rm EW}$. In the expansions, we assume the large $\tan\beta$ limit and take $m_b\tan\beta \sim \mathcal{O}(M_{\rm EW})$. This expansion has been studied in detail for the decay $h \to b\bar{b}$, with particular emphasis on the decoupling properties of the results as M_S and $M_{\tilde{g}} \to \infty$ [28]. The SQCD contributions to the decay, $h \to b\bar{b}$, extracted from our results are in agreement with those of Refs. [28,42].

The final result for maximal mixing, summing all contributions, is

$$\begin{aligned}
A_s &\equiv -g_sT^Ag_{bbh}M_s^\mu\left\{1 + \frac{\alpha_s(\mu_R)}{4\pi}X_i^s\right\} \\
&= -g_sT^Ag_{bbh}M_s^\mu\left\{1 + \left(\frac{\delta g_{bbh}}{g_{bbh}}\right)_{\rm max} + \frac{\alpha_s(\mu_R)}{4\pi}\frac{s}{M_S^2}\delta\kappa_{\rm max}\right\}, \\
A_t &\equiv -g_sT^Ag_{bbh}M_s^\mu\left\{1 + \frac{\alpha_s(\mu_R)}{4\pi}X_i^t\right\} \\
&= -g_sT^Ag_{bbh}M_t^\mu\left\{1 + \left(\frac{\delta g_{bbh}}{g_{bbh}}\right)_{\rm max}\right\}, \\
A_1 &\equiv -g_sT^Ag_{bbh}M_s^\mu\left\{1 + \frac{\alpha_s(\mu_R)}{4\pi}X_i^1\right\} \\
&= -g_sT^Ag_{bbh}M_1^\mu\left(-\frac{\alpha_s(\mu_R)u}{2\pi M_S^2}\right)\delta\kappa_{\rm max}.
\end{aligned} \tag{37}$$

The contribution, which is a rescaling of the $b\bar{b}h$ vertex, is

$$\left(\frac{\delta g_{bbh}}{g_{bbh}}\right)_{\rm max} = \left(\frac{\delta g_{bbh}}{g_{bbh}}\right)_{\rm max}^{(1)} + \left(\frac{\delta g_{bbh}}{g_{bbh}}\right)_{\rm max}^{(2)}, \tag{38}$$

where the leading order term in $M_{\rm EW}/M_S$ is $\mathcal{O}(1)$,

$$\left(\frac{\delta g_{bbh}}{g_{bbh}}\right)_{\rm max}^{(1)} = \frac{\alpha_s(\mu_R)}{3\pi}\frac{M_{\tilde{g}}(X_b - Y_b)}{M_S^2}f_1(R), \tag{39}$$

with $Y_b \equiv A_b + \mu\cot\alpha$ and $R \equiv M_{\tilde{g}}/M_S$. Equation (39) only decouples for large M_S if the additional limit $M_A \to \infty$ is also taken [23,28]. In this limit,

$$X_b - Y_b \to \frac{2\mu M_Z^2}{M_A^2}\tan\beta\cos 2\beta + \mathcal{O}\left(\frac{M_{\rm EW}^4}{M_A^4}\right). \tag{40}$$

The subleading terms of $\mathcal{O}(M_{\rm EW}^2/M_S^2)$ are[8]

$$\begin{aligned}
\left(\frac{\delta g_{bbh}}{g_{bbh}}\right)_{\rm max}^{(2)} = \frac{\alpha_s(\mu_R)}{3\pi}\Bigg\{&-\frac{M_{\tilde{g}}Y_b}{M_S^2}\left[\frac{M_h^2}{12M_S^2}f_3^{-1}(R) + \frac{X_b^2m_b^2}{2(1+\Delta_b)^2M_S^4}f_3(R)\right] \\
&- \frac{m_b^2X_bY_b}{2(1+\Delta_b)^2M_S^4}f_3^{-1}(R) + \frac{M_Z^2}{3M_S^2}\frac{c_\beta s_{\alpha+\beta}}{s_\alpha}I_3^b \\
&\times\left[3f_1(R) + \left(\frac{2M_{\tilde{g}}X_b}{M_S^2} - 1\right)f_2(R)\right]\Bigg\}.
\end{aligned} \tag{41}$$

The functions $f_i(R)$ are defined in Appendix C.

The $\frac{s}{M_S^2}$, $\frac{u}{M_S^2}$ terms in Eq. (37) are not a rescaling of the lowest order vertex and cannot be obtained from the effective Lagrangian. We find

[8] We use the shorthand $c_\beta = \cos\beta$, $s_{\alpha+\beta} = \sin(\alpha+\beta)$, etc.

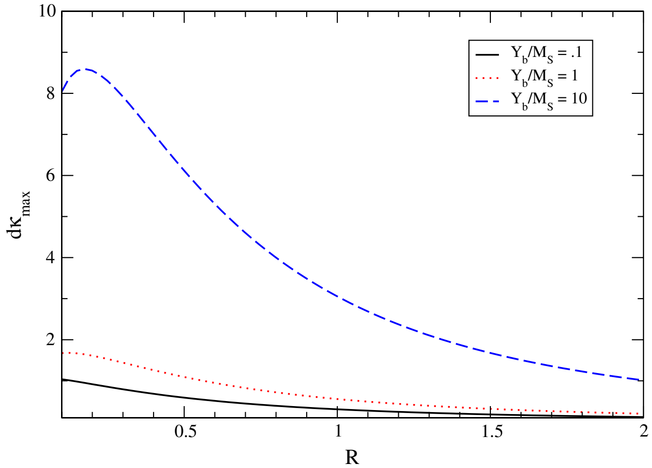

FIG. 2 (color online). Contribution of $\delta\kappa_{\max}$ defined in Eq. (42) as a function of $R = M_{\tilde{g}}/M_S$.

$$\delta\kappa_{\max} = \frac{1}{4}\left[f_3(R) + \frac{1}{9}f_3^{-1}(R)\right] - R\frac{Y_b}{2M_S}\left[f_2'(R) + \frac{1}{9}\hat{f}_2(R)\right]. \tag{42}$$

The $\delta\kappa_{\max}$ term is $\mathcal{O}(1)$ in $M_{\rm EW}/M_S$ and has its largest values for small R and large ratios of Y_b/M_S, as can be seen in Fig. 2. Large effects can be obtained for $Y_b/M_S \sim 10$ and $M_{\tilde{g}} \ll M_S$. However, the parameters must be carefully tuned so that $A_b/M_S \lesssim 1$ in order not to break color [45].

The amplitude squared, summing over final state spins and colors and averaging over initial state spins and colors, including one-loop SQCD corrections, is

$$|\bar{\mathcal{A}}|^2_{\max} = -\frac{2\pi\alpha_s(\mu_R)}{3}g_{bbh}^2\left[\left(\frac{u^2+M_h^4}{st}\right)\left[1+2\left(\frac{\delta g_{bbh}}{g_{bbh}}\right)_{\max}\right] + \frac{\alpha_s(\mu_R)}{2\pi}\frac{M_h^2}{M_S^2}\delta\kappa_{\max}\right]. \tag{43}$$

Note that in the cross section, the $\delta\kappa_{\max}$ term is not enhanced by a power of s and it gives a contribution of $\mathcal{O}(\frac{M_{\rm EW}^2}{M_S^2})$.

Expanding Δ_b in the maximal mixing limit,

$$\Delta_b \to -\frac{\alpha_s(\mu_S)}{3\pi}\frac{M_{\tilde{g}}\mu}{M_S^2}\tan\beta f_1(R) + \mathcal{O}\left(\frac{M_{\rm EW}^4}{M_S^4}\right). \tag{44}$$

By comparison with Eq. (14),

$$|\bar{\mathcal{A}}|^2_{\max} = -\frac{2\pi\alpha_s(\mu_R)}{3}(g_{bbh}^{\Delta_b})^2\left\{\left(\frac{u^2+M_h^4}{st}\right)\left[1 + 2\left(\frac{\delta g_{bbh}}{g_{bbh}}\right)^{(2)}_{\max}\right] + \frac{\alpha_s(\mu_R)}{2\pi}\frac{M_h^2}{M_S^2}\delta\kappa_{\max}\right\} + \mathcal{O}\left(\left[\frac{M_{EW}}{M_S}\right]^4, \alpha_s^3\right). \tag{45}$$

Note that the mismatch in the arguments of α_s in Eqs. (44) and (45) is higher order in α_s than the terms considered here. The $(\delta g_{bbh}/g_{bbh})^{(2)}_{\max}$ and $\delta\kappa_{\max}$ terms both correspond to contributions which are not present in the effective Lagrangian approach. These terms are, however, suppressed by powers of $M_{\rm EW}^2/M_S^2$, and the nondecoupling effects discussed in Refs. [27,28] are completely contained in the $g_{bbh}^{\Delta_b}$ term.

B. Minimal mixing in the b-squark sector

The minimal mixing scenario is characterized by a mass splitting between the b squarks, which is of order the b-squark mass, $|M^2_{\tilde{b}_1} - M^2_{\tilde{b}_2}| \sim M_S^2$. In this case,

$$|\tilde{m}_L^2 - \tilde{m}_R^2| \gg \frac{m_b|X_b|}{(1+\Delta_b)}, \tag{46}$$

and the mixing angle in the b-squark sector is close to zero,

$$\cos 2\tilde{\theta}_b \sim 1 - \frac{2m_b^2X_b^2}{(M^2_{\tilde{b}_1} - M^2_{\tilde{b}_2})^2}\left(\frac{1}{1+\Delta_b}\right)^2. \tag{47}$$

The nonzero subamplitudes are

$$A_s = -g_sT^Ag_{bbh}M_s^\mu\left\{1 + \left(\frac{\delta g_{bbh}}{g_{bbh}}\right)_{\min} + \frac{\alpha_s(\mu_R)}{4\pi}\frac{s}{\tilde{M}_g^2}\delta\kappa_{\min}\right\},$$
$$A_t = -g_sT^Ag_{bbh}M_t^\mu\left\{1 + \left(\frac{\delta g_{bbh}}{g_{bbh}}\right)_{\min}\right\},$$
$$A_1 = -g_sT^Ag_{bbh}M_1^\mu\left(-\frac{\alpha_s(\mu_R)u}{2\pi\tilde{M}_g^2}\right)\delta\kappa_{\min}. \tag{48}$$

Expanding the exact one-loop results of Appendix B in the minimal mixing scenario,

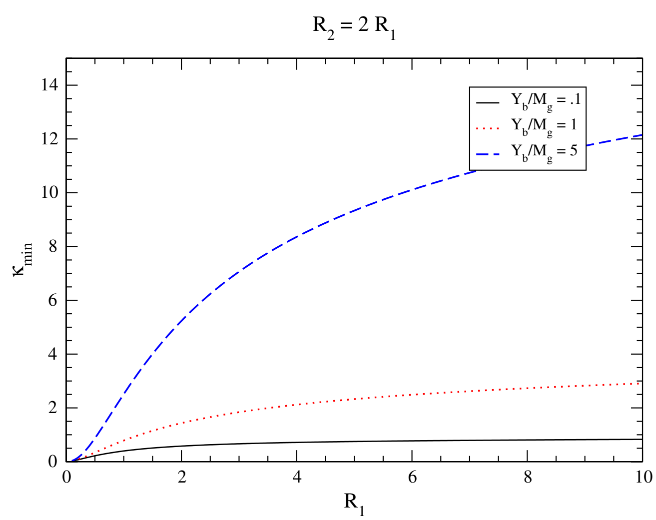

FIG. 3 (color online). Contribution of $\delta\kappa_{\min}$ defined in Eq. (49) as a function of $R_i = M_{\tilde{g}}/M_{\tilde{b}_i}$.

$$\delta\kappa_{\min} = \frac{1}{8}\Sigma_{i=1}^{2}\left(R_i^2\left[\frac{1}{9}f_3^{-1}(R_i) + f_3(R_i)\right]\right) + \frac{Y_b}{M_{\tilde g}}\frac{R_1^2R_2^2}{R_2^2 - R_1^2}\left(3h_1(R_1, R_2, 1) + \frac{8}{3}h_1(R_1, R_2, 2)\right), \tag{49}$$

where $R_i = M_{\tilde g}/M_{\tilde b_i}$ and the functions $f_i(R_i)$ and $h_i(R_1, R_2, n)$ are defined in Appendix C. The $\delta\kappa_{\min}$ function is shown in Fig. 3. For large values of $Y_b/M_{\tilde g}$ it can be significantly larger than 1.

As in the previous section, the spin and color averaged amplitude squared is

$$|\bar A|^2_{\min} = -\frac{2\alpha_s(\mu_R)\pi}{3}(g_{bbh}^2)\left\{\frac{(M_h^4 + u^2)}{st}\left[1 + 2\left(\frac{\delta g_{bbh}}{g_{bbh}}\right)_{\min}\right] + \frac{\alpha_s(\mu_R)}{2\pi}\delta\kappa_{\min}\frac{M_h^2}{M_{\tilde g}^2}\right\}, \tag{50}$$

with

$$\left(\frac{\delta g_{bbh}}{g_{bbh}}\right)_{\min} = \left(\frac{\delta g_{bbh}}{g_{bbh}}\right)^{(1)}_{\min} + \left(\frac{\delta g_{bbh}}{g_{bbh}}\right)^{(2)}_{\min}. \tag{51}$$

The leading order term in $M_{\rm EW}/M_S$ is $\mathcal{O}(1)$,

$$\left(\frac{\delta g_{bbh}}{g_{bbh}}\right)^{(1)}_{\min} = \frac{2\alpha_s(\mu_R)}{3\pi}\frac{(X_b - Y_b)}{M_{\tilde g}}\frac{R_1^2R_2^2}{R_1^2 - R_2^2}h_1(R_1, R_2, 0). \tag{52}$$

The subleading terms are $\mathcal{O}(\frac{M_{\rm EW}^2}{M_S^2})$,

$$\begin{aligned}\left(\frac{\delta g_{bbh}}{g_{bbh}}\right)^{(2)}_{\min} = \frac{\alpha_s}{4\pi}\Bigg\{&-\frac{8M_{\tilde g}Y_b}{3\Delta M^2_{\tilde b_{12}}}\left[\frac{h_2(R_1, R_2)M_h^2}{\Delta M^2_{\tilde b_{12}}} + \frac{m_b^2X_b^2}{(\Delta M^2_{\tilde b_{12}})^2(1 + \Delta_b)^2}\left\{2\mathcal{S}\left(\frac{f_1(R)}{M_{\tilde b}^2}\right) + \frac{h_1(R_1, R_2, 0)}{\Delta M^2_{\tilde b_{12}}}\right\}\right]\\
&+\frac{4}{3}\frac{c_\beta s_{\alpha+\beta}}{s_\alpha}I_3^bM_Z^2\left[\mathcal{S}\left(\frac{3f_1(R) - f_2(R)}{3M_{\tilde b}^2}\right) - \frac{2M_{\tilde g}X_b}{\Delta M^2_{\tilde b_{12}}}\mathcal{A}\left(\frac{f_1(R)}{M_{\tilde b}^2}\right)\right]\\
&+\frac{4}{3}\frac{c_\beta s_{\alpha+\beta}}{s_\alpha}(I_3^b - 2Q^bs_W^2)M_Z^2\left[\mathcal{A}\left(\frac{3f_1(R) - f_2(R)}{3M_{\tilde b}^2}\right) - \frac{2M_{\tilde g}X_b}{\Delta M^2_{\tilde b_{12}}}\left\{\mathcal{S}\left(\frac{f_1(R)}{M_{\tilde b}^2}\right) + \frac{h_1(R_1, R_2, 0)}{\Delta M^2_{\tilde b_{12}}}\right\}\right]\\
&+\frac{8}{3}\frac{m_b^2X_bY_b}{\Delta M^2_{\tilde b_{12}}(1 + \Delta_b)^2}\mathcal{A}\left(\frac{3f_1(R) - f_2(R)}{3M_{\tilde b}^2}\right)\Bigg\}.\end{aligned} \tag{53}$$

The symmetric and antisymmetric functions are defined as

$$\begin{aligned}\mathcal{S}(f(R, M_{\tilde b}) &\equiv \tfrac{1}{2}[f(R_1, M_{\tilde b_1}) + f(R_2, M_{\tilde b_2})],\\ \mathcal{A}(f(R, M_{\tilde b}) &\equiv \tfrac{1}{2}[f(R_1, M_{\tilde b_1}) - f(R_2, M_{\tilde b_2})]\end{aligned} \tag{54}$$

and $\Delta M^2_{\tilde b_{12}} \equiv M^2_{\tilde b_1} - M^2_{\tilde b_2}$. The remaining functions are defined in Appendix C.

By expanding Δ_b in the minimal mixing limit, we find the analogous result to that of the maximal mixing case,

$$|\bar A|^2_{\min} = -\frac{2\alpha_s\pi}{3}(g^{\Delta_b}_{bbh})^2\left\{\frac{(M_h^4 + u^2)}{st}\left[1 + 2\left(\frac{\delta g_{bbh}}{g_{bbh}}\right)^{(2)}_{\min}\right] + \frac{\alpha_s}{2\pi}\delta\kappa_{\min}\frac{M_h^2}{M_{\tilde g}^2}\right\} + \mathcal{O}\left(\left[\frac{M_{\rm EW}}{M_S}\right]^4, \alpha_s^3\right). \tag{55}$$

The contributions which are not contained in $\sigma_{\rm IBA}$ are again found to be suppressed by $\mathcal{O}([\frac{M_{\rm EW}}{M_S}]^2)$.

IV. NUMERICAL RESULTS

We present results for $pp \to b(\bar b)h$ at $\sqrt{s} = 7$ TeV with $p_{Tb} > 20$ GeV and $|\eta_b| < 2.0$. We use FEYNHIGGS to generate M_h and $\sin\alpha_{\rm eff}$ and then iteratively solve for the b-squark masses and Δ_b from Eqs. (12) and (19). We evaluate the two-loop $\overline{\rm MS}$ b mass at $\mu_R = M_h/2$, which we also take to be the renormalization and factorization scales.[9] Finally, Figs. 4–7 use the CTEQ6m NLO parton distribution functions [46]. Figures 4–6 show the percentage deviation of the complete one-loop SQCD calculation from the improved Born approximation of Eq. (16) for $\tan\beta = 40$ and $\tan\beta = 20$ and representative values of the MSSM parameters.[10] In both extremes of b-squark mixing, the improved Born approximation is within a few percent of the complete one-loop SQCD calculation and so is a reliable prediction for the rate. This is true for both large and small M_A. In addition, the large M_S expansion accurately reproduces the full SQCD one-loop result to within a few percent. These results are expected from the expansions of Eqs. (45) and (55), since the terms which differ between the improved Born approximation and the one-loop calculation are suppressed in the large M_S limit.

[9] Δ_b is evaluated using $\alpha_s(M_S)$.

[10] Figures 4–6 do not include the pure QCD NLO corrections [18].

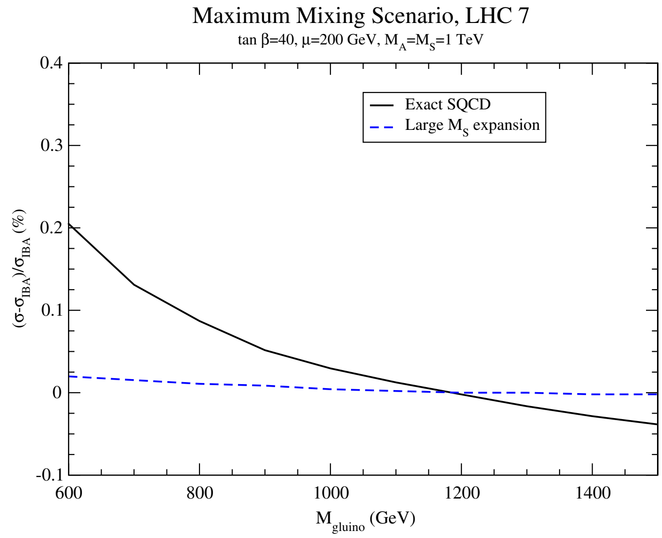

FIG. 4 (color online). Percentage difference between the improved Born approximation and the exact one-loop SQCD calculation of $pp \rightarrow bh$ for maximal mixing in the b-squark sector at $\sqrt{s} = 7$ TeV, $\tan\beta = 40$, and $M_A = 1$ TeV.

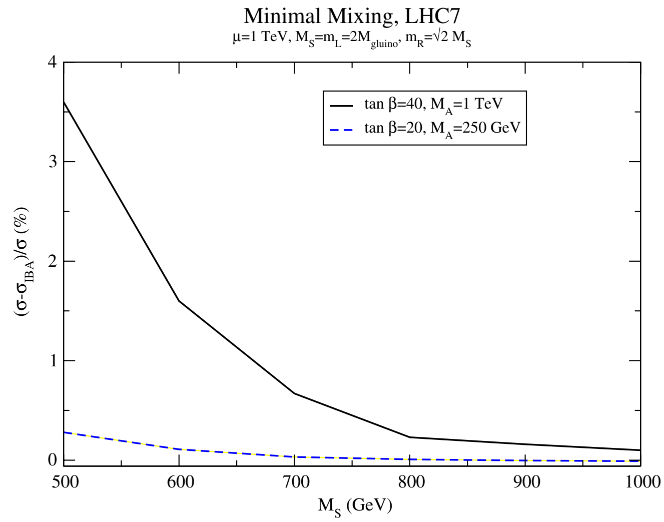

FIG. 6 (color online). Percentage difference between the improved Born approximation and the exact one-loop SQCD calculation for $pp \rightarrow bh$ for minimal mixing in the b-squark sector at $\sqrt{s} = 7$ TeV.

Figure 7 compares the total SQCD rate for maximal and minimal mixing, which brackets the allowed mixing possibilities. For large M_S, the effect of the mixing is quite small, while for $M_S \sim 800$ GeV, the mixing effects are at most a few fb. The accuracy of the improved Born approximation as a function of m_R is shown in Fig. 8 for fixed M_A, μ, and m_L. As m_R is increased, the effects become very tiny. Even for light gluino masses, the improved Born approximation reproduces the exact SQCD result to within a few percent.

In Fig. 9, we show the scale dependence for the total rate, including NLO QCD and SQCD corrections (dotted lines) for a representative set of MSSM parameters at $\sqrt{s} = 7$ TeV. The NLO scale dependence is quite small when $\mu_R = \mu_F \sim M_h$. However, there is roughly $\sim 5\%$ difference between the predictions found using the CTEQ6m parton distribution functions (PDFs) and the MSTW2008 NLO PDFs [47]. In Fig. 10, we show the scale dependence for small μ_F (as preferred by [17]), and see that it is significantly larger than in Fig. 9. This is consistent with the results of [4,29].

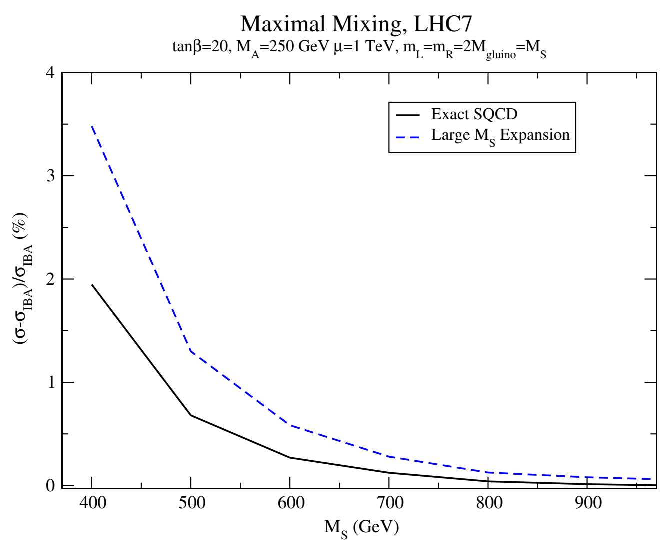

FIG. 5 (color online). Percentage difference between the improved Born approximation and the exact one-loop SQCD calculation of $pp \rightarrow bh$ for maximal mixing in the b-squark sector at $\sqrt{s} = 7$ TeV, $\tan\beta = 20$, and $M_A = 250$ GeV.

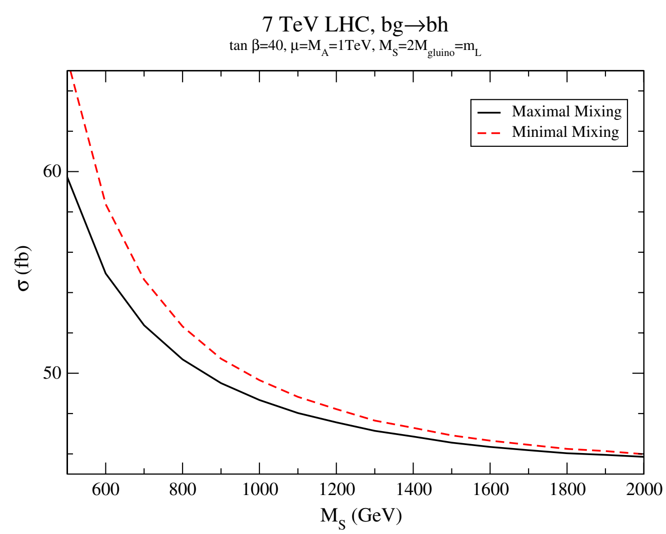

FIG. 7 (color online). Comparison between the exact one-loop SQCD calculation for $pp \rightarrow bh$ for minimal and maximal mixing in the b-squark sector at $\sqrt{s} = 7$ TeV and $\tan\beta = 40$. The minimal mixing curve has $m_R = \sqrt{2}M_S$ and $\tilde{\theta}_b \sim 0$, while the maximal mixing curve has $m_R = M_S$ and $\tilde{\theta}_b \sim \frac{\pi}{4}$.

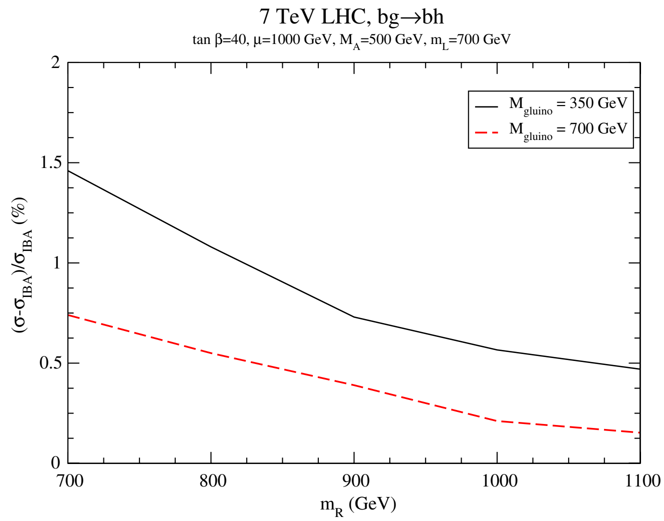

FIG. 8 (color online). Percentage difference between the improved Born approximation and the exact one-loop SQCD calculation for $pp \to bh$ as a function of m_R at $\sqrt{s} = 7$ TeV and $\tan\beta = 40$.

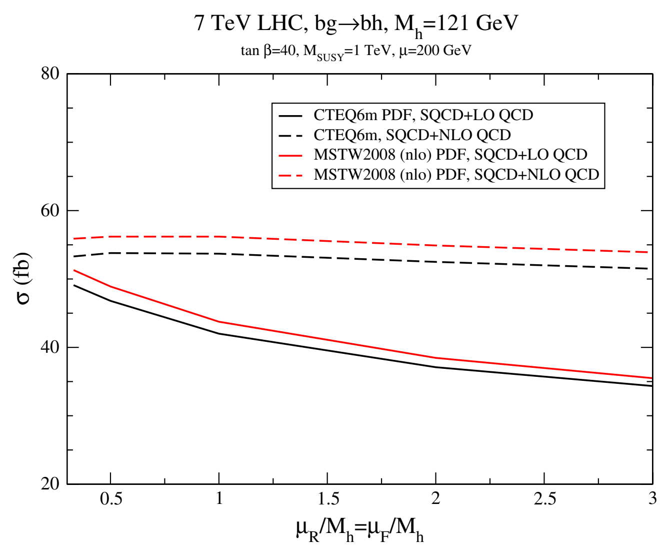

FIG. 9 (color online). Total cross section for $pp \to b(\bar{b})h$ production, including NLO QCD and SQCD corrections (dotted lines), as a function of the renormalization/factorization scale using CTEQ6m (black solid line) and MSTW2008 NLO (red dashed line) PDFs. We take $M_{\tilde{g}} = 1$ TeV and the remaining MSSM parameters as in Fig. 4.

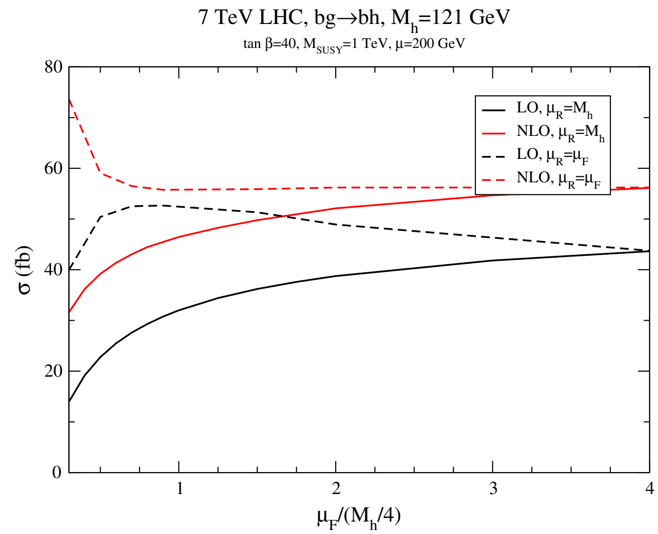

FIG. 10 (color online). Total cross section for $pp \to b(\bar{b})h$ production, including NLO QCD and SQCD corrections, as a function of the factorization scale using MSTW2008 NLO PDFs. We take $M_{\tilde{g}} = 1$ TeV and the remaining MSSM parameters as in Fig. 4.

V. CONCLUSION

Our major results are the analytic expressions for the SQCD corrections to b Higgs associated production in the minimal [Eqs. (41), (42), and (45)] and maximal [Eqs. (49), (53), and (55)] b-squark mixing scenarios for large $\tan\beta$ and squark masses, M_S. These results clearly demonstrate that deviations from the Δ_b approximation are suppressed by powers of $(M_{\rm EW}/M_S)$ in the large $\tan\beta$ region. The Δ_b approximation hence yields an accurate prediction in the five-flavor number scheme for the cross section for squark and gluino masses at the TeV scale. As a by-product of our calculation, we update the predictions for b Higgs production at $\sqrt{s} = 7$ TeV.

ACKNOWLEDGMENTS

S. Dawson and P. Jaiswal are supported by the U.S. Department of Energy under Grant No. DE-AC02-98CH10886.

APPENDIX A: PASSARINO-VELTMAN FUNCTIONS

The scalar integrals are defined as

$$
\begin{aligned}
\frac{i}{16\pi^2} A_0(M_0^2) &= \int \frac{d^n k}{(2\pi)^n} \frac{1}{N_0}, \\
\frac{i}{16\pi^2} B_0(p_1^2; M_0^2, M_1^2) &= \int \frac{d^n k}{(2\pi)^n} \frac{1}{N_0 N_1}, \\
\frac{i}{16\pi^2} C_0(p_1^2, p_2^2, (p_1+p_2)^2; M_0^2, M_1^2, M_2^2) &= \int \frac{d^n k}{(2\pi)^n} \frac{1}{N_0 N_1 N_2}, \\
\frac{i}{16\pi^2} D_0(p_1^2, p_2^2, p_3^2, p_4^2, (p_1+p_2)^2, (p_2+p_3)^2; M_0^2, M_1^2, M_2^2, M_3^2) &= \int \frac{d^n k}{(2\pi)^n} \frac{1}{N_0 N_1 N_2 N_3},
\end{aligned}
\tag{A1}
$$

where

$$\begin{aligned} N_0 &= k^2 - M_0^2, \\ N_1 &= (k+p_1)^2 - M_1^2, \\ N_2 &= (k+p_1+p_2)^2 - M_2^2, \\ N_3 &= (k+p_1+p_2+p_3)^2 - M_3^2. \end{aligned} \tag{A2}$$

The tensor integrals encountered are expanded in terms of the external momenta p_i and the metric tensor $g^{\mu\nu}$. For the two-point function we write

$$\frac{i}{16\pi^2} B^\mu(p_1^2; M_0^2, M_1^2) = \int \frac{d^n k}{(2\pi)^n} \frac{k^\mu}{N_0 N_1} \equiv \frac{i}{16\pi^2} p_1^\mu B_1(p_1^2, M_0^2, M_1^2), \tag{A3}$$

while for the three-point functions we have both rank-one and rank-two tensor integrals which we expand as

$$\begin{aligned} &C^\mu(p_1^2, p_2^2, (p_1+p_2)^2; M_0^2, M_1^2, M_2^2) = p_1^\mu C_{11} + p_2^\mu C_{12}, \\ &C^{\mu\nu}(p_1^2, p_2^2, (p_1+p_2)^2; M_0^2, M_1^2, M_2^2) \\ &\quad = p_1^\mu p_1^\nu C_{21} + p_2^\mu p_2^\nu C_{22} + (p_1^\mu p_2^\nu + p_1^\nu p_2^\mu) C_{23} + g^{\mu\nu} C_{24}, \end{aligned} \tag{A4}$$

where

$$\frac{i}{16\pi^2} C^\mu(C^{\mu\nu})(p_1^2, p_2^2, (p_1+p_2)^2; M_0^2, M_1^2, M_2^2) \equiv \int \frac{d^n k}{(2\pi)^n} \frac{k^\mu (k^\mu k^\nu)}{N_0 N_1 N_2}. \tag{A5}$$

Finally, for the box diagrams, we encounter rank-one and rank-two tensor integrals which are written in terms of the Passarino-Veltman coefficients as

$$\begin{aligned} &\frac{i}{16\pi^2} D^\mu(p_1^2, p_2^2, p_3^2, p_4^2, (p_1+p_2)^2, (p_2+p3)^2; M_0^2, M_1^2, M_2^2) \\ &\quad \equiv \int \frac{d^n k}{(2\pi)^n} \frac{k^\mu}{N_0 N_1 N_2 N_3} \\ &\quad = \frac{i}{16\pi^2} \{p_1^\mu D_{11} + p_2^\mu D_{12} + p_3^\mu D_{13}\}, \end{aligned} \tag{A6}$$

$$\begin{aligned} &\frac{i}{16\pi^2} D^{\mu\nu}(p_1^2, p_2^2, p_3^2, p_4^2, (p_1+p_2)^2, (p_2+p_3)^2; M_0^2, M_1^2, M_2^2) \\ &\quad \equiv \int \frac{d^n k}{(2\pi)^n} \frac{k^\mu k^\nu}{N_0 N_1 N_2 N_3} \\ &\quad = \frac{i}{16\pi^2} \{g^{\mu\nu} D_{00} + \text{tensor structures not needed here}\}. \end{aligned} \tag{A7}$$

APPENDIX B: ONE-LOOP RESULTS

In this appendix we give the nonzero contributions of the individual diagrams in terms of the basis functions of Eq. (20) and the decompositions of Eq. (22). The contributions proportional to $m_b \tan\beta$ are new and were not included in the results of Ref. [23]. Although we specialize to the case of the lightest Higgs boson, h, our results are easily generalized to the heavier neutral Higgs boson, H, and so the Feynman diagrams in this appendix are shown for $\phi_i = h, H$.

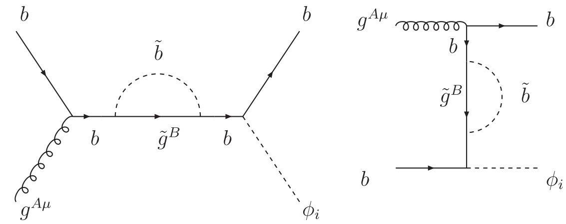

FIG. 11. Self-energy diagrams S_1 and S_2.

The self-energy diagrams of Fig. 11 show

$$\begin{aligned} X_{S_1}^{(t)} &= \frac{4}{3} \sum_{i=1}^{2} \left\{ B_1 - (-1)^i \frac{2 m_b M_{\tilde g} s_{2\tilde b}}{t} B_0 \right\} (M_{\tilde b_i}^2), \\ X_{S_1}^{(2)} &= -\frac{4}{3} \sum_{i=1}^{2} (-1)^i \frac{m_b M_{\tilde g} s_{2\tilde b}}{t} B_0(M_{\tilde b_i}^2), \end{aligned} \tag{B1}$$

where we have used the shorthand notation for the arguments of Passarino-Veltman functions, $B_{0,1}(M_{\tilde b_i}^2) \equiv B_{0,1}(t; M_{\tilde g}^2, M_{\tilde b_i}^2)$.

$$\begin{aligned} X_{S_2}^{(s)} &= \frac{4}{3} \sum_{i=1}^{2} \left\{ B_1 - (-1)^i \frac{2 m_b M_{\tilde g} s_{2\tilde b}}{s} B_0 \right\} (M_{\tilde b_i}^2), \\ X_{S_2}^{(2)} &= -\frac{4}{3} \sum_{i=1}^{2} (-1)^i \frac{m_b M_{\tilde g} s_{2\tilde b}}{s} B_0(M_{\tilde b_i}^2), \end{aligned} \tag{B2}$$

and $B_{0,1}(M_{\tilde b_i}^2) \equiv B_{0,1}(s; M_{\tilde g}^2, M_{\tilde b_i}^2)$.

The vertex functions of Fig. 12 are as follows.

Diagram V_1:

$$\begin{aligned} X_{V_1}^{(s)} &= \frac{s}{6} \sum_{i=1}^{2} \left\{ C_{12} + C_{23} - (-1)^i \frac{2 m_b M_{\tilde g} s_{2\tilde b}}{t} (C_0 + C_{11}) \right\} \\ &\quad \times (M_{\tilde b_i}^2), \\ X_{V_1}^{(t)} &= -\frac{1}{6} \sum_{i=1}^{2} \{ t(C_{12} + C_{23}) + 2C_{24} \\ &\quad - (-1)^i 2 m_b M_{\tilde g} s_{2\tilde b} (C_0 + C_{11}) \} (M_{\tilde b_i}^2), \\ X_{V_1}^{(1)} &= -\frac{u}{3} \sum_{i=1}^{2} \left\{ C_{12} + C_{23} - (-1)^i \frac{2 m_b M_{\tilde g} s_{2\tilde b}}{t} (C_0 + C_{11}) \right\} \\ &\quad \times (M_{\tilde b_i}^2), \\ X_{V_1}^{(3)} &= -\frac{1}{3} \sum_{i} (-1)^i m_b M_{\tilde g} s_{2\tilde b} (C_0 + C_{11}) (M_{\tilde b_i}^2), \end{aligned} \tag{B3}$$

where $C_{0,11,12,23,24}(M_{\tilde b_i}^2) \equiv C_{0,11,12,23,24}(0, 0, t; M_{\tilde g}^2, M_{\tilde b_i}^2, M_{\tilde b_i}^2)$.

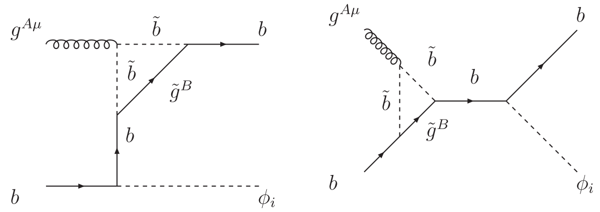

FIG. 12. Virtual diagrams V_1 and V_2.

Diagram V_2:

$$X^{(s)}_{V_2} = -\frac{1}{3}\sum_{i=1}^{2} C_{24}(M^2_{\tilde{b}_i}),$$

$$X^{(1)}_{V_2} = -\frac{u}{3}\sum_{i=1}^{2}\left\{C_{12} + C_{23} - (-1)^i \frac{2m_b M_{\tilde{g}} s_{2\tilde{b}}}{s}(C_0 + C_{11})\right\} \times (M^2_{\tilde{b}_i}),$$

$$X^{(4)}_{V_2} = \frac{1}{3}\sum_{i}(-1)^i m_b M_{\tilde{g}} s_{2\tilde{b}}(C_0 + C_{11})(M^2_{\tilde{b}_i}), \tag{B4}$$

where $C_{0,11,12,23,24}(M^2_{\tilde{b}_i}) \equiv C_{0,11,12,23,24}(0,0,s;M^2_{\tilde{g}},M^2_{\tilde{b}_i},M^2_{\tilde{b}_i})$.

The vertex functions of Fig. 13 are as follows.

Diagram V_3:

$$X^{(s)}_{V_3} = \frac{3s}{2}\sum_{i=1}^{2}\left\{C_{12} + C_{23} - (-1)^i \frac{2m_b M_{\tilde{g}} s_{2\tilde{b}}}{t}(C_0 + C_{12})\right\} \times (M^2_{\tilde{b}_i}),$$

$$X^{(t)}_{V_3} = -\frac{3}{2}\sum_{i=1}^{2}\{M^2_{\tilde{g}}C_0 - 2(1-\epsilon)C_{24} - (-1)^i 2m_b M_{\tilde{g}} s_{2\tilde{b}} C_{12}\} \times (M^2_{\tilde{b}_i}),$$

$$X^{(1)}_{V_3} = -3u\sum_{i=1}^{2}\{C_{12} + C_{23} - (-1)^i \frac{2m_b M_{\tilde{g}} s_{2\tilde{b}}}{t}(C_0 + C_{12})\} \times (M^2_{\tilde{b}_i}),$$

$$X^{(2)}_{V_3} = -\frac{3}{2}\sum_{i=1}^{2}(-1)^i m_b M_{\tilde{g}} s_{2\tilde{b}} C_0(M^2_{\tilde{b}_i}),$$

$$X^{(3)}_{V_3} = -3\sum_{i=1}^{2}(-1)^i m_b M_{\tilde{g}} s_{2\tilde{b}}\{C_0 + C_{12}\}(M^2_{\tilde{b}_i}), \tag{B5}$$

where $C_{0,11,12,23,24}(M^2_{\tilde{b}_i}) \equiv C_{0,11,12,23,24}(0,0,t;M^2_{\tilde{g}},M^2_{\tilde{g}},M^2_{\tilde{b}_i})$.

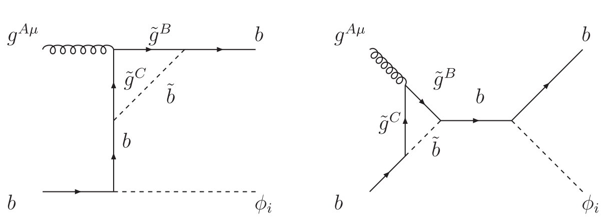

FIG. 13. Virtual diagrams V_3 and V_4.

Diagram V_4:

$$X^{(s)}_{V_4} = -\frac{3}{2}\sum_{i=1}^{2}\{M^2_{\tilde{g}}C_0 - 2(1-\epsilon)C_{24} - s(C_{12} + C_{23}) + (-1)^i 2m_b M_{\tilde{g}} s_{2\tilde{b}} C_0\}(M^2_{\tilde{b}_i}),$$

$$X^{(1)}_{V_4} = -3u\sum_{i=1}^{2}\{C_{12} + C_{23} - (-1)^i \frac{2m_b M_{\tilde{g}} s_{2\tilde{b}}}{s}(C_0 + C_{12})\} \times (M^2_{\tilde{b}_i}),$$

$$X^{(2)}_{V_4} = -\frac{3}{2}\sum_{i=1}^{2}(-1)^i m_b M_{\tilde{g}} s_{2\tilde{b}} C_0(M^2_{\tilde{b}_i}),$$

$$X^{(4)}_{V_4} = 3\sum_{i=1}^{2}(-1)^i m_b M_{\tilde{g}} s_{2\tilde{b}}\{C_0 + C_{12}\}(M^2_{\tilde{b}_i}), \tag{B6}$$

where $C_{0,11,12,23,24}(M^2_{\tilde{b}_i}) \equiv C_{0,11,12,23,24}(0,0,s;M^2_{\tilde{g}},M^2_{\tilde{g}},M^2_{\tilde{b}_i})$.

The vertex functions of Fig. 14 are as follows.

Diagram V_5:

$$X^{(t)}_{V_5} = \frac{4}{3}\sum_{i,j=1}^{2} C_{h,ij}\{\delta_{ij} m_b C_{11} + a_{ij} M_{\tilde{g}} C_0\}(M^2_{\tilde{b}_i}, M^2_{\tilde{b}_j}),$$

$$X^{(2)}_{V_5} = \frac{4}{3} m_b \sum_{i,j=1,2} C_{h,ij}\delta_{ij} C_{12}(M^2_{\tilde{b}_i}, M^2_{\tilde{b}_j}), \tag{B7}$$

where $C_{0,11,12,23,24}(M^2_{\tilde{b}_i}, M^2_{\tilde{b}_j}) \equiv C_{0,11,12,23,24}(0, M^2_h, t; M^2_{\tilde{g}}, M^2_{\tilde{b}_i}, M^2_{\tilde{b}_j})$, the squark mixing matrix is defined as

$$\begin{pmatrix} a_{11} & a_{12} \\ a_{21} & a_{22} \end{pmatrix} = \begin{pmatrix} s_{2\tilde{b}} & c_{2\tilde{b}} \\ c_{2\tilde{b}} & -s_{2\tilde{b}} \end{pmatrix}, \tag{B8}$$

and the light Higgs-squark-squark couplings $C_{h,ij}$ are normalized with respect to the Higgs-quark-quark coupling [2],

$$C_{h,11} + C_{h,22} = 4m_b + \frac{2M_Z^2}{m_b} I_3^b \frac{s_{\alpha+\beta}c_\beta}{s_\alpha}, \tag{B9}$$

$$C_{h,11} - C_{h,22} = 2Y_b s_{2\tilde{b}} + \frac{2M_Z^2}{m_b} c_{2\tilde{b}}(I_3^b - 2Q_b s_W^2)\frac{s_{\alpha+\beta}c_\beta}{s_\alpha}, \tag{B10}$$

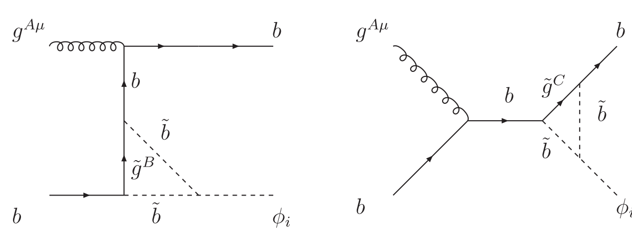

FIG. 14. Virtual diagrams V_5 and V_6.

$$C_{h,12} = C_{h,21} = Y_b c_{2\tilde{b}} - \frac{M_Z^2}{m_b} s_{2\tilde{b}} (I_3^b - 2Q^b s_W^2) \frac{s_{\alpha+\beta} c_\beta}{s_\alpha}, \tag{B11}$$

$s_W^2 = \sin\theta_W^2 = 1 - M_W^2/M_Z^2$, and Y_b is defined below Eq. (41).

Diagram V_6:

$$\begin{aligned}
X_{V_6}^{(s)} &= \frac{4}{3} \sum_{i,j=1,2} C_{h,ij} \{\delta_{ij} m_b C_{11} + a_{ij} M_{\tilde{g}} C_0\}(M_{\tilde{b}_i}^2, M_{\tilde{b}_j}^2), \\
X_{V_6}^{(2)} &= \frac{4}{3} m_b \sum_{i,j=1,2} C_{h,ij} \delta_{ij} C_{12}(M_{\tilde{b}_i}^2, M_{\tilde{b}_j}^2), \\
X_{V_6}^{(t)} &= X_{V_6}^{(3)} = X_{V_6}^{(4)} = 0,
\end{aligned} \tag{B12}$$

where $C_{0,11,12,23,24}(M_{\tilde{b}_i}^2, M_{\tilde{b}_j}^2) \equiv C_{0,11,12,23,24}(0, M_h^2, s; M_{\tilde{g}}^2, M_{\tilde{b}_i}^2, M_{\tilde{b}_j}^2)$.

The box diagram of Fig. 15 shows

$$\begin{aligned}
X_{B_1}^{(s)} &= \frac{3M_{\tilde{g}} s}{2} \sum_{i,j=1,2} a_{ij} C_{h,ij} \{D_0 + D_{13}\}(M_{\tilde{b}_i}^2, M_{\tilde{b}_j}^2), \\
X_{B_1}^{(t)} &= -\frac{3M_{\tilde{g}} t}{2} \sum_{i,j=1,2} a_{ij} C_{h,ij} D_{13}(M_{\tilde{b}_i}^2, M_{\tilde{b}_j}^2), \\
X_{B_1}^{(1)} &= 3M_{\tilde{g}} u \sum_{i,j=1,2} a_{ij} C_{h,ij} \{D_{11} - D_{13}\}(M_{\tilde{b}_i}^2, M_{\tilde{b}_j}^2), \\
X_{B_1}^{(2)} &= -\frac{3m_b}{2} \sum_{i,j=1,2} \delta_{ij} C_{h,ij} \{M_{\tilde{g}}^2 D_0 - 2D_{00}\}(M_{\tilde{b}_i}^2, M_{\tilde{b}_j}^2),
\end{aligned} \tag{B13}$$

where $D_0(M_{\tilde{b}_i}^2, M_{\tilde{b}_j}^2) \equiv D_0(0,0,0,M_h^2,s,t; M_{\tilde{b}_i}^2, M_{\tilde{g}}^2, M_{\tilde{g}}^2, M_{\tilde{b}_j}^2)$.

The box diagram B_2 of Fig. 16 shows

$$\begin{aligned}
X_{B_2}^{(s)} &= -\frac{M_{\tilde{g}} s}{6} \sum_{i,j=1,2} a_{ij} C_{h,ij} \{D_0 + D_{11}\}(M_{\tilde{b}_i}^2, M_{\tilde{b}_j}^2), \\
X_{B_2}^{(t)} &= \frac{M_{\tilde{g}} t}{6} \sum_{i,j=1,2} a_{ij} C_{h,ij} \{D_0 + D_{11}\}(M_{\tilde{b}_i}^2, M_{\tilde{b}_j}^2), \\
X_{B_2}^{(1)} &= \frac{M_{\tilde{g}} u}{3} \sum_{i,j=1,2} a_{ij} C_{h,ij} \{D_{11} - D_{12}\}(M_{\tilde{b}_i}^2, M_{\tilde{b}_j}^2), \\
X_{B_2}^{(2)} &= -\frac{m_b}{3} \sum_{i,j=1,2} \delta_{ij} C_{h,ij} D_{00}(M_{\tilde{b}_i}^2, M_{\tilde{b}_j}^2),
\end{aligned} \tag{B14}$$

where $D_0(M_{\tilde{b}_i}^2, M_{\tilde{b}_j}^2) \equiv D_0(0, 0, 0, M_h^2, u, s; M_{\tilde{b}_i}^2, M_{\tilde{g}}^2, M_{\tilde{b}_j}^2, M_{\tilde{b}_j}^2)$.

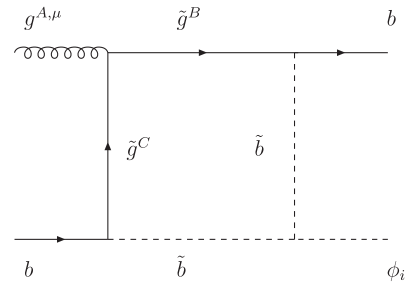

FIG. 15. Box diagram B_1.

The box diagram B_3 of Fig. 17 shows

$$\begin{aligned}
X_{B_3}^{(s)} &= \frac{M_{\tilde{g}} s}{6} \sum_{i,j=1,2} a_{ij} C_{h,ij} \{D_0 + D_{12}\}(M_{\tilde{b}_i}^2, M_{\tilde{b}_j}^2), \\
X_{B_3}^{(t)} &= -\frac{M_{\tilde{g}} t}{6} \sum_{i,j=1,2} a_{ij} C_{h,ij} \{D_0 + D_{12}\}(M_{\tilde{b}_i}^2, M_{\tilde{b}_j}^2), \\
X_{B_3}^{(1)} &= \frac{M_{\tilde{g}} u}{3} \sum_{i,j=1,2} a_{ij} C_{h,ij} \{D_{11} - D_{12}\}(M_{\tilde{b}_i}^2, M_{\tilde{b}_j}^2), \\
X_{B_3}^{(2)} &= -\frac{m_b}{3} \sum_{i,j=1,2} \delta_{ij} C_{h,ij} D_{00}(M_{\tilde{b}_i}^2, M_{\tilde{b}_j}^2),
\end{aligned} \tag{B15}$$

where $D_0(M_{\tilde{b}_i}^2, M_{\tilde{b}_j}^2) \equiv D_0(0, 0, 0, M_h^2, u, t; M_{\tilde{b}_i}^2, M_{\tilde{g}}^2, M_{\tilde{b}_j}^2, M_{\tilde{b}_j}^2)$.

The vertex and external wave function counterterms, Eq. (29), along with the subtraction of Eq. (32), give the counterterm of Eq. (33):

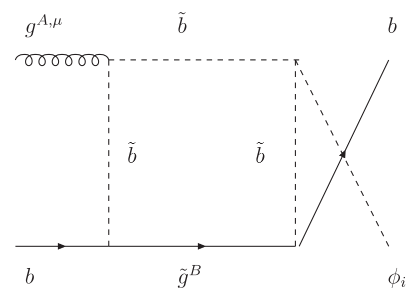

FIG. 16. Box diagram B_2.

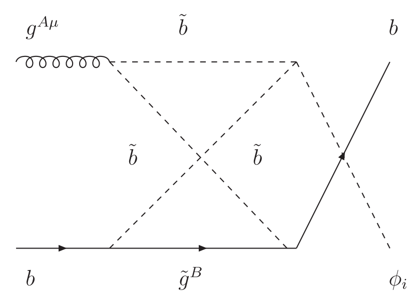

FIG. 17. Box diagram B_3.

$$X_{\rm CT}^{(s)} = X_{\rm CT}^{(t)} = \left(\frac{4\pi}{\alpha_s(\mu_R)}\right)\left[\delta Z_b^V + \frac{\delta m_b}{m_b} + \delta_{\rm CT}\right]$$
$$= \frac{4}{3}\left[2M_{\tilde g} Y_b I(M_{\tilde b_1}, M_{\tilde b_2}, M_{\tilde g}) + \sum_{i=1}^{2}(-(-1)^i 2m_b s_{2\tilde b} B_0' + 2m_b^2 B_1')(0; M_{\tilde g}^2, M_{\tilde b_i}^2)\right]. \tag{B16}$$

Note that the counterterm contains no large $\tan\beta$ enhanced contribution.

APPENDIX C: DEFINITIONS

In this appendix we define the functions used in the expansions of the Passarino-Veltman integrals in the maximum and minimum mixing scenarios, where $R \equiv \frac{M_{\tilde g}}{M_S}$ in the maximal mixing scenario, and $R_i \equiv \frac{M_{\tilde b_i}}{M_S}$ in the minimal mixing scenario:

$$f_1(R) = \frac{2}{(1-R^2)^2}[1 - R^2 + R^2 \log R^2], \qquad f_2(R) = \frac{3}{(1-R^2)^3}[1 - R^4 + 2R^2 \log R^2],$$
$$f_3(R) = \frac{4}{(1-R^2)^4}\left[1 + \frac{3}{2}R^2 - 3R^4 + \frac{1}{2}R^6 + 3R^2 \log R^2\right],$$
$$f_4(R) = \frac{5}{(1-R^2)^5}\left[\frac{1}{2} - 4R^2 + 4R^6 - \frac{1}{2}R^8 - 6R^4 \log R^2\right],$$
$$h_1(R_1, R_2, n) = \left(\frac{R_1^2}{1-R_1^2}\right)^n \frac{\log R_1^2}{1-R_1^2} - \left(\frac{R_2^2}{1-R_2^2}\right)^n \frac{\log R_2^2}{1-R_2^2} - \sum_{j=0}^{n}(-1)^j \frac{j+2}{2}\{(1-R_1^2)^{j-n} - (1-R_2^2)^{j-n}\},$$
$$h_2(R_1, R_2) = \frac{R_1^2 + R_2^2 - 2}{(1-R_1^2)(1-R_2^2)} + \frac{1}{R_1^2 - R_2^2}\left[\frac{R_1^2 + R_2^2 - 2R_1^4}{(1-R_1^2)^2}\log R_1^2 - \frac{R_1^2 + R_2^2 - 2R_2^4}{(1-R_2^2)^2}\log R_2^2\right]. \tag{C1}$$

Further,

$$f_i'(R) \equiv \frac{df_i(x)}{dx^2}\bigg|_{x=R}, \qquad f_i^{-1}(R) \equiv \frac{f_i(1/R)}{R^2}, \qquad \hat f_i(R) \equiv \frac{1}{R^4}\frac{df_i(x)}{dx^2}\bigg|_{x=1/R}. \tag{C2}$$

[1] A. Djouadi, Phys. Rep. **459**, 1 (2008).
[2] J. F. Gunion, H. E. Haber, G. L. Kane, and S. Dawson, *The Higgs Hunter's Guide* (Addison Wesley, Menlo Park, 1990).
[3] M. S. Carena and H. E. Haber, Prog. Part. Nucl. Phys. **50**, 63 (2003).
[4] S. Dittmaier *et al.* (LHC Higgs Cross Section Working Group), arXiv:1101.0593.
[5] D. Benjamin *et al.* (Tevatron New Phenomena and Higgs Working Group), arXiv:1003.3363.
[6] S. Chatrchyan *et al.* (CMS Collaboration), arXiv:1104.1619.
[7] G. Aad *et al.* (ATLAS Collaboration), arXiv:0901.0512.
[8] G. L. Bayatian *et al.* (CMS Collaboration), J. Phys. G **34**, 995 (2007).
[9] S. Dawson, C. B. Jackson, L. Reina, and D. Wackeroth, Phys. Rev. Lett. **94**, 031802 (2005).
[10] S. Dawson, C. B. Jackson, L. Reina, and D. Wackeroth, Mod. Phys. Lett. A **21**, 89 (2006).
[11] M. S. Carena, A. Menon, and C. E. M. Wagner, Phys. Rev. D **76**, 035004 (2007).
[12] J. Campbell *et al.*, arXiv:hep-ph/0405302.
[13] S. Dittmaier, M. Kramer, and M. Spira, Phys. Rev. D **70**, 074010 (2004).
[14] M. S. Carena, S. Mrenna, and C. E. M. Wagner, Phys. Rev. D **60**, 075010 (1999).
[15] S. Dawson, C. B. Jackson, L. Reina, and D. Wackeroth, Phys. Rev. D **69**, 074027 (2004).
[16] F. Maltoni, Z. Sullivan, and S. Willenbrock, Phys. Rev. D **67**, 093005 (2003).
[17] F. Maltoni, T. McElmurry, and S. Willenbrock, Phys. Rev. D **72**, 074024 (2005).
[18] D. Dicus, T. Stelzer, Z. Sullivan, and S. Willenbrock, Phys. Rev. D **59**, 094016 (1999).
[19] J. Campbell, R. K. Ellis, F. Maltoni, and S. Willenbrock, Phys. Rev. D **67**, 095002 (2003).
[20] B. Field, L. Reina, and C. B. Jackson, Phys. Rev. D **76**, 074008 (2007).
[21] S. Dawson and P. Jaiswal, Phys. Rev. D **81**, 073008 (2010).
[22] M. Beccaria *et al.*, Phys. Rev. D **82**, 093018 (2010).
[23] S. Dawson and C. B. Jackson, Phys. Rev. D **77**, 015019 (2008).
[24] A. Dabelstein, Nucl. Phys. **B456**, 25 (1995).

[25] L. J. Hall, R. Rattazzi, and U. Sarid, Phys. Rev. D **50**, 7048 (1994).

[26] M. S. Carena, D. Garcia, U. Nierste, and C. E. M. Wagner, Nucl. Phys. **B577**, 88 (2000).

[27] J. Guasch, P. Hafliger, and M. Spira, Phys. Rev. D **68**, 115001 (2003).

[28] H. E. Haber *et al.*, Phys. Rev. D **63**, 055004 (2001).

[29] R. V. Harlander and W. B. Kilgore, Phys. Rev. D **68**, 013001 (2003).

[30] S. Heinemeyer, W. Hollik, H. Rzehak, and G. Weiglein, Eur. Phys. J. C **39**, 465 (2005).

[31] A. Brignole, G. Degrassi, P. Slavich, and F. Zwirner, Nucl. Phys. **B643**, 79 (2002).

[32] D. Noth and M. Spira, arXiv:1001.1935.

[33] D. Noth and M. Spira, Phys. Rev. Lett. **101**, 181801 (2008).

[34] S. Dittmaier, M. Kramer, A. Muck, and T. Schluter, J. High Energy Phys. 03 (2007) 114.

[35] S. Heinemeyer, W. Hollik, and G. Weiglein, Comput. Phys. Commun. **124**, 76 (2000).

[36] G. Degrassi, S. Heinemeyer, W. Hollik, P. Slavich, and G. Weiglein, Eur. Phys. J. C **28**, 133 (2003).

[37] S. Heinemeyer, W. Hollik, and G. Weiglein, Eur. Phys. J. C **9**, 343 (1999).

[38] M. S. Carena, M. Olechowski, S. Pokorski, and C. E. M. Wagner, Nucl. Phys. **B426**, 269 (1994).

[39] S. Dittmaier, M. Kramer, M. Spira, and M. Walser, Phys. Rev. D **83**, 055005 (2011).

[40] E. L. Berger, T. Han, J. Jiang, and T. Plehn, Phys. Rev. D **71**, 115012 (2005).

[41] L. Hofer, U. Nierste, and D. Scherer, J. High Energy Phys. 10 (2009) 081.

[42] E. Accomando, G. Chachamis, F. Fugel, M. Spira, and M. Walser, arXiv:1103.4283.

[43] S. Berge, W. Hollik, W. M. Mosle, and D. Wackeroth, Phys. Rev. D **76**, 034016 (2007).

[44] P. Nason, S. Dawson, and R. K. Ellis, Nucl. Phys. **B303**, 607 (1988).

[45] J. F. Gunion, H. E. Haber, and M. Sher, Nucl. Phys. **B306**, 1 (1988).

[46] P. M. Nadolsky *et al.*, Phys. Rev. D **78**, 013004 (2008).

[47] A. D. Martin, W. J. Stirling, R. S. Thorne, and G. Watt, Eur. Phys. J. C **63**, 189 (2009).